Science Bulletin 64 (2019) 896–903

Contents lists available at ScienceDirect

Science Bulletin

journal homepage: www.elsevier.com/locate/scib

Science Bulletin
www.scibull.com

Article

Enhancement of the degradation ability for organic pollutants via the synergistic effect of photoelectrocatalysis on a self-assembled perylene diimide (SA-PDI) thin film

Hong Miao [a], Jun Yang [a], Guilong Peng [b], Huiquan Li [c], Yongfa Zhu [a,c,*]

[a] Department of Chemistry, Tsinghua University, Beijing 100084, China
[b] School of Environment, Beijing Key Laboratory for Emerging Organic Contaminants Control, State Key Joint Laboratory of Environment Simulation and Pollution Control (SKLESPC), Tsinghua University, Beijing 100084, China
[c] Anhui Provincical Key Laboratory for Degradation and Monitoring of Pollution of the Environment, School of Chemistry and Materials Engineering, Fuyang Normal University, Fuyang 236037, China

ARTICLE INFO

Article history:
Received 22 March 2019
Received in revised form 28 April 2019
Accepted 6 May 2019
Available online 11 May 2019

Keywords:
Photoelectrocatalytic oxidation
PDI electrode
Phenol
Degradation

ABSTRACT

A self-assembled perylene diimide (SA-PDI) film was prepared on an indium-tin-oxide (ITO) substrate and acted as a photoanode for the photoelectrocatalytic (PEC) degradation of some emerging contaminants under visible light irradiation ($\lambda > 420$ nm) and applied voltage. Due to the synergistic effect, the photocatalytic degradation rate by the SA-PDI film under visible light irradiation and an applied voltage of 2.1 V was 2.72 times and 14.5 times those of the PC and EC processes, respectively. The visible light irradiation not only generated a promoting effect on electrocatalytic (EC) oxidation at potentials above 1.2 V but also generated many more h^+ for promoting the electrocatalytic oxidation of phenol. Furthermore, an applied voltage above 1.2 V could effectively improve the separation rate of electrons from the SA-PDI electrodes to the Pt electrodes, and then, much more $\cdot O_2^-$ and ·OH could be generated for improving the photocatalytic (PC) oxidation efficiency. Therefore, the h^+, ·OH and $\cdot O_2^-$ could improve the synergistic effect of phenol oxidation during the PEC process. Moreover, the SA-PDI film appeared to have satisfactory stability in the PEC process. The SA-PDI film was also proven to be effective for two other contaminants, namely, 2,4-dichlorophenol, and ciprofloxacin.

1. Introduction

Coking wastewater contains many poisonous substances, such as polycyclic aromatic hydrocarbons, volatile phenol and other heterocyclic compounds. It is generated from coal gas purification and coal coking [1]. These poisonous substances are mutagenic, carcinogenic and refractory. They could cause harmful pollution problems and lead to the serious toxicity of coking wastewater to the entire world [2]. More seriously, phenolic compounds have exhibited low biodegradability. Therefore, the phenolic compounds discharged into natural water could pose a harmful and persistent threat to our human health. In many industrial enterprises, phenol is a common by-product and intermediate chemical material. Since it is a strong irritant and highly toxic, phenol is considered to be a priority pollutant and needs to be controlled. Traditional methods such as extraction, biological treatment and chemical oxidation have been used to purify the phenolic wastewater [3–8]. All of them have a large energy consumption, low mineralization or secondary pollution. These defects have limited their use in practical applications. Thus, there is an urgent goal to develop some new methods for phenol degradation.

Photocatalysis (PC) has been widely used in organic contaminant degradation in the last 20 years [9–11]. The photocatalyst can produce some highly active species under light irritation. The active species could be used to oxidize some phenolic compounds at ambient temperature and pressure. At the same time, PC is low-cost, environmentally friendly and highly efficient [12]. However, PC also has some shortcomings such as its low utilization of solar energy and rapid recombination of h^+ and e^-, which limit its photocatalytic degradation efficiency [13]. Moreover, the powder catalyst is very difficult to separate and recycle from the water [14].

With the increasing demand for clean energy and the growing problem of water pollution, the photoelectrocatalytic (PEC) technique has been regarded as a promising approach for the effective removal of refractory pollutants due to the fast separation of

* Corresponding author.
E-mail address: zhuyf@mail.tsinghua.edu.cn (Y. Zhu).

https://doi.org/10.1016/j.scib.2019.05.006
2095-9273/

charge carriers conducted by applying an external potential [15–22]. The most investigated photoanode material is TiO_2. It can utilize ultraviolet light to achieve the efficient degradation of various organic pollutants [23–25]. To make the most of the solar light, more visible-light-responsive semiconductors such as WO_3 [26], $BiVO_4$ [27–29], and Fe_2O_3 [30] have been developed. However, most of the semiconductors were inorganic semiconductors or contain metallic elements, which are difficult to degrade. Therefore, to address this problem, developing suitable organic semiconductors has become a major obstacle for the practical application of the PEC process.

In recent years, our group had performed much research on organic semiconductor materials. Especially, a perylene diimide (PDI) supramolecular organic photocatalyst that acted as a special n-type nanomaterial was formed through the self-assembly of PDI molecules. Due to the high charge carrier mobility and electron affinity, it could be widely used in the degradation of organic pollutants under visible light irradiation [31–35]. Some significant methods such as copolymerization [36], doping [37], supermolecular assembly [33], and surface heterojunction design [38–40] have been reported for increasing the catalytic activity. Although PDI has excellent visible light absorption compared with other photocatalysts, it is difficult to achieve effective degradation and deep mineralization for phenol using the pure photocatalyst. Therefore, the photocatalysis of PDI nanomaterials could be combined with electrochemical oxidation to enhance the catalytic activity of PDI. This synergistic photoelectric effect is beneficial to enhance the degradation of phenol.

In the present work, the self-assembled PDI (SA-PDI) electrode was synthesized in two simple steps. First, the bulk perylene diimide (PDI) was dissolved in alkaline solution and then self-assembled in the acidic solution to obtain a PDI nanowire. Then, the PDI nanomaterials were immobilized onto the ITO substrate and formed the SA-PDI electrode. The formation of the SA-PDI film significantly promoted the separation of the photogenerated hole-electron pairs under visible light irradiation ($\lambda > 420$ nm) and applied voltage. Phenol, a strong irritant and highly toxic organic contaminant, was chosen as the target pollutant to investigate the PEC activity of the SA-PDI electrode (Scheme 1). At the same time, the enhanced mechanism of the degradation process has also been discussed.

2. Experimental

All chemicals were analytical-grade reagents and purchased from the Aladdin Chemical Reagent Co., Ltd. The indium-tin-oxide (ITO) glass was purchased from the China Southern Glass Co., Ltd. The size of the ITO was 20 mm × 40 mm, and the thickness was 1.1 mm. The resistance of the ITO sheet was 22 Ω/square.

2.1. Preparation of electrodes

The bulk PDI and PDI nanomaterials were obtained by the reported method, which is elaborated in the supporting document.

The SA-PDI electrodes were prepared through the dip coating method. In brief, a certain quality of as-synthesized PDI nanowire was dissolved in 5 mL of ethanol with strong stirring for 30 min. Then, the slurry was coated onto the 20 mm × 40 mm ITO glass electrode. The prepared SA-PDI electrode was conducted at 120 °C for 2 h. Finally, half of the PDI nanomaterial on the ITO glass was removed leaving an approximately 20 mm × 20 mm PDI film on the ITO glass. The as-synthesized electrode was washed with pure water and dried before use. The obtained electrode was denoted as a SA-PDI film. The bulk PDI was also used to prepare an electrode through the above-methods and denoted as a B-PDI film.

2.2. Characterization

The morphology of the as-synthesized electrode was researched by transmission electron microscopy (TEM, Hitachi HT7700) and scanning electron microscopy (SEM, Hitachi SU-8010). The UV–Vis diffuse reflection spectra (UV–Vis/DRS) of the samples were investigated by a UV–Vis spectrophotometer (Hitachi U-3010). The chemical state and elemental composition of the obtained electrode were tested by X-ray photoelectron spectroscopy (XPS, ULVAC-PHI, Quantera). A Perkin-Elmer LS55 spectrophotometer was used to record the fluorescence spectra of the films. The main active species during the PC, EC, and PEC processes were detected by electron paramagnetic resonance spectrometry (EPR, JES-FA200). A Bruker V70 spectrometer was applied to measure the Fourier transform infrared (FT-IR) spectrum of the PDI nanowire. The visible light was provided by a 500 W xenon lamp ($\lambda > 420$ nm, Institute for Electric Light Sources, Beijing). The photoelectrochemical tests were studied using a three-electrode system, which included a saturated calomel electrode (SCE), working electrode (as-prepared film electrodes), and counter electrode (Pt wire). The electrolyte solution was 0.1 mol/L Na_2SO_4. The frequency range in the electrochemical impedance spectra (EIS) tests was 0.1–100,000 Hz. The potential range of 0–1.3 V was applied in the cyclic voltammetry (CV) scans, for which the scan rate was 0.1 V/s. The photoluminescence (PL) spectra of the SA-PDI and B-PDI were tested and compared under an excitation wavelength of 600 nm.

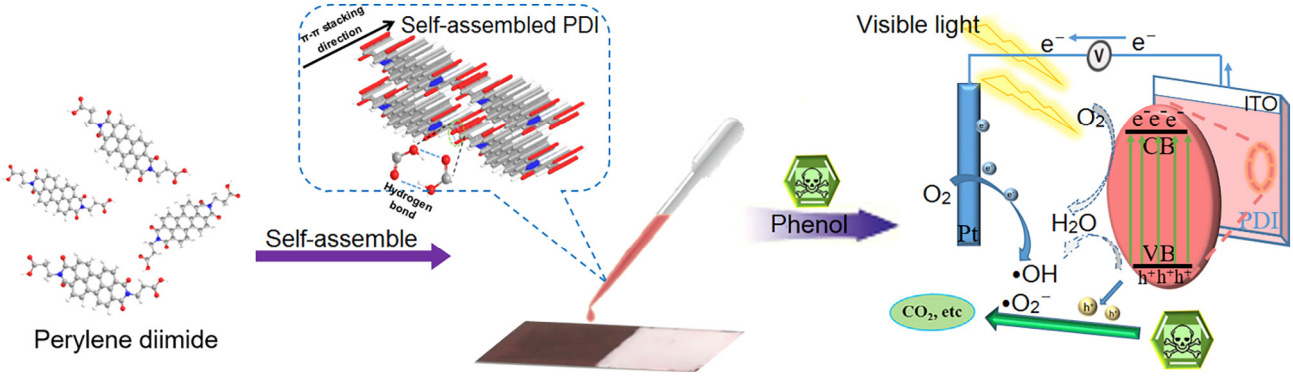

Scheme 1. (Color online) Schematic illustration of PDI films with highly phenol degradation under the PEC process.

2.3. Photoelectrocatalytic degradation of phenol

The degradation processes were tested using the abovementioned three-electrode system. The pH of the electrolyte was regulated by phosphate buffered solution (PBS, 0.1 mol/L). Phenol was the degradation molecular probe. The visible light was obtained from a 500 W xenon lamp equipped with a 420 nm cut-off filter. The average light intensity was 35 mW/cm^2. A potential range of 0–2.4 V was employed for the PEC study.

2.4. Analytical methods

The concentration of phenol during the PEC process was detected by HPLC with a UV absorbance detector at 270 nm (Agela Technologies Inc.). The reversed phase column was a Venusil XBP-C18. The mobile phase was CH_3OH and H_2O (55:45, v:v), for which the flow rate was 1 mL/min. The experimental methods in the EC and PC processes are the same as those described above without the applied voltage or visible light.

3. Results and discussion

3.1. Morphology and structure

The morphologies of as-prepared Bulk PDI and self-assembled PDI nanowire were observed by TEM (Fig. 1c and f). The length of the PDI nanowire was 100–300 nm, and the diameter was approximately 20 nm (Fig. 1f). Fig. 1a and d shows the SEM images of the B-PDI film and SA-PDI film, respectively. It can be seen that the SA-PDI film was much denser and smaller than the B-PDI film, which could improve the contact surface between the self-assembled PDI and the pollutant. The thickness of the film was nearly 200 nm (Fig. 1b and e).

The FT-IR spectroscopy was used to confirm the functional groups of the prepared PDI nanowires (Fig. S1a online). The FT-IR data of the PDI nanowires showed that peaks at 1,652 and 1,688 cm^{-1} belonged to the C=O stretching, indicating the ketone functionalities in the perylene diimide molecular structure and carboxyl structure. The stretching vibration at 1,590 cm^{-1} could be attributed to the σ C=C groups from the aromatic carbon skeleton. Correspondingly, the Raman spectra of bulk PDI and the self-assembled PDI nanowire exhibited peaks at 1,394 and 1,590 cm^{-1}, respectively (Fig. S1b online) [41]. It is hard to observe the difference between the PDI nanowire and bulk PDI. These results, along with the FT-IR spectroscopy analysis, confirmed that the structure of the PDI nanowire was similar to that of bulk PDI. The crystalline phase of the obtained films was identified by X-ray diffraction (XRD) technology (Fig. S1c online). In addition, The PDI nanowire had a high degree of crystallinity and small d-spacing for π-π stacking, which is expected to benefit the migration of charge carriers [41]. Furthermore, the XPS spectra (Fig. S1d online) were also employed to analyse the groups in detail. The narrow spectra of O 1s, C 1s and N 1s analyses further confirmed that multiple functional groups were shown on the surface of the PDI nanowires (Fig. S2 online).

3.2. Optical properties

Fig. S3 (online) shows the UV–Vis/DRS spectra of the SA-PDI and B-PDI films. It was found that the absorption edge of the SA-PDI film was wider than that of the B-PDI film. The obvious redshift indicated that the SA-PDI film might exhibit superior PEC performance. The Tauc plot could be used to estimate the band gap energies of the B-PDI and SA-PDI films (Eq. (1)):

$$(\alpha h\upsilon)^2 = A(h\upsilon - E_g), \quad (1)$$

where, α is the absorption coefficient, $h\upsilon$ is the photon energy and A is a constant. Therefore, the band gap energies (E_g) of the SA-PDI and B-PDI films could be estimated easily by the Tauc plot $(\alpha h\upsilon)^2 = 0$ [42]. Based on the intercept of the linear section, the band gap energy of the SA-PDI film was 1.748 eV, which is lower than that of the B-PDI film (1.811 eV) (Fig. S3a online). Therefore, the narrow band gap could be beneficial for the separation of the photogenerated hole-electron pairs. Next, the PL spectra of the B-PDI and SA-PDI films were measured to investigate the recombination rate of the h^+-e^- carriers (Fig. S3b online). The fluorescence emission spectra (655–820 nm) of samples were measured at a confirmed excitation wavelength (600 nm). It is worth noting that the

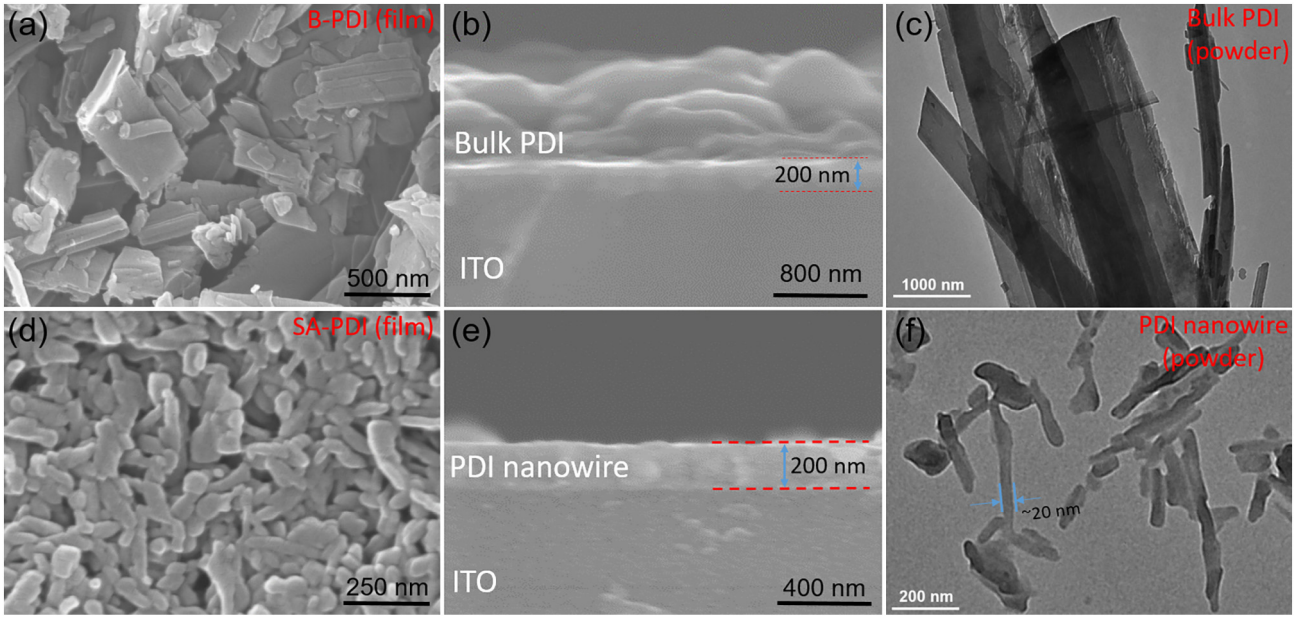

Fig. 1. (Color online) Top-view SEM images of B-PDI (a) and SA-PDI (d) films; the side-view SEM images of B-PDI (b) and SA-PDI (e) films; and the TEM images of bulk PDI (c) and the PDI nanowires (f).

fluorescence intensity of the SA-PDI film was lower than that of the B-PDI film, which indicates that the SA-PDI film had a lower recombination rate of holes and electrons. These results, along with the morphology, confirmed that the SA-PDI film could significantly reduce the recombination of the photogenerated charge carriers, resulting in excellent PEC activity.

3.3. Photoelectochemical properties

In the process of the photoelectrocatalytic degradation of phenol, the separation of photogenerated h^+-e^- pairs was very important. Therefore, some effective techniques such as electrochemical impedance spectroscopy (EIS) measurements, photocurrent tests, and linear sweep voltammograms (LSV) were used to study the carrier separation efficiency of the SA-PDI film. The photocurrent response of the SA-PDI film was much higher than that of the B-PDI film under the visible light irradiation (Fig. 2). The enhanced photocurrent response of the SA-PDI film indicated that the SA-PDI electrode had a better separation efficiency of photogenerated carriers than the B-PDI electrode (Fig. 2a). Furthermore, the photocurrent response could also be enhanced by the applied voltage (Fig. 2b). Thus, the photoelectrocatalytic performance was improved due to the effects of the visible light and applied voltage. Similarly, the separation efficiency of the h^+-e^- pairs and the interfacial charge transfer resistance could also be reflected by the radius of the circular arc [43,44]. The arc radius decreased gradually as the applied voltage of the SA-PDI film increased (Fig. S4 online). As we all know, an increase in the Faraday capacitance constant could decrease the impedance generated from the Faraday current at the same frequency. At the same time, the energy barrier that the electrode reaction needed to overcome decreased. Thus, the reactions could easily occur on the electrode. Significantly, the photoelectrochemical data of the SA-PDI film indicated that the catalytic reaction rate of the phenol degradation could be improved by increasing the applied voltage and the visible light irradiation.

The CV scans of the SA-PDI film in the Na_2SO_4 solution (0.1 mol/L) with phenol (5 ppm) were also tested (Fig. 3). As shown in Fig. 3a, the current intensity of the CV curve was reduced as time goes by. When the SA-PDI film was washed by water, the current intensity could be recovered and was higher than the third CV curve (Fig. 3b). These results indicated that the phenol could be polymerized and easily formed a polymer film on the surface of the PDI/ITO electrode, which led to the passivation of the SA-PDI film. When the applied voltage increased to 1.2 V, water molecules on the electrode surface were oxidized and decomposed, producing more active substances, such as $\cdot O_2^-$ and ·OH [45,46]. Thus, the degradation rate of phenol was enhanced.

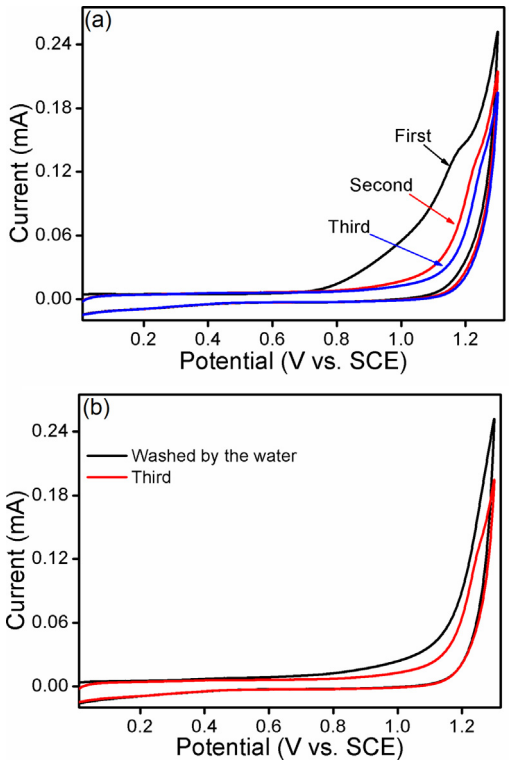

Fig. 3. (Color online) The CV scans of the SA-PDI film in a Na_2SO_4 (0.1 mol/L) electrolyte with phenol (5 ppm). (a) The CV curves of 3 times recycled tests. (b) The CV curves of the SA-PDI film before and after washed by the water.

3.4. Photoelectooxidation performance of phenol

First, the photoelectrocatalytic stabilities of the SA-PDI film in alkaline (pH 7.4) and acidic (pH 5.6) environments were studied. As illustrated in Fig. S5 (online), the colour of the reaction solution became red as the time progressed when the SA-PDI film was in the alkaline (pH 7.4) environment, which was due to the depolymerisation of the PDI nanowire during the cooperative photoelectric degradation of organic pollutants [47]. Thus, further different processes for phenol degradation were tested in the acidic solution (pH 5.6).

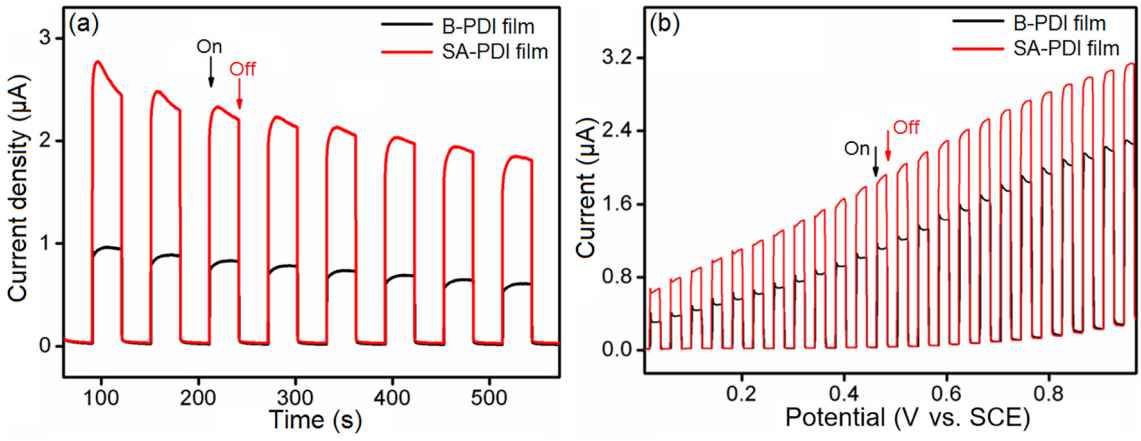

Fig. 2. (Color online) Photocurrent response curves (a) and LSV plots (b) of B-PDI and SA-PDI films under visible light irradiation and dark.

The phenol degradation tests of the B-PDI and SA-PDI films in the PC and PEC processes are shown in Fig. S6 (online). The corresponding slope of the fitting line is equal to the kinetic constant k [48,49], which could be used to compare the catalytic performances. The PEC degradation rate constant of the SA-PDI film was 0.087 h^{-1} under visible light irradiation and an applied voltage of 2.1 V, which was 2.72 times higher than that at 0 V (0.032 h^{-1}) (Fig. 4a). The PC degradation efficiency of phenol by the SA-PDI film was greatly increased with an applied voltage of 2.1 V (Fig. S6 online). Comparing the degradation performance in the PC and PEC processes, the applied voltage could reduce the recombination of the e^--h^+ pairs and produce more $\cdot O_2^-$ and ·OH. Thus, the PC activity of the SA-PDI film was enhanced by the applied voltage (Fig. S6a and b online). On the other hand, the degradation activity of phenol in the EC process with an external potential of 2.1 V was only 0.006 h^{-1}, which was much lower than that of the PEC process. The visible light irradiation generated a promoting effect for EC oxidation. The PEC, EC, and PC degradation rates of the B-PDI film were also measured (Fig. 4b) to explain the synergistic effect of photoelectrocatalysis for phenol degradation.

3.5. Effect of the applied voltage

In the PEC degradation, the applied voltage could transfer the photogenerated electrons to the Pt electrode and prevent the recombination of the electron-hole pairs. The effect of the applied voltage (0–2.4 V vs. SCE.) for phenol degradation was investigated on a SA-PDI film (Fig. 4c) and B-PDI film (Fig. S7 online). The results showed that when the applied voltage increased from 0 to 2.1 V, the degradation of phenol increased significantly. The satisfactory degradation performance was due to the enhanced separation of the e^--h^+ pairs with increasing applied voltage. However, the amount of electrons generated by the fixed visible light irradiation is constant. Thus, the width of the layer was difficult to further increase if the applied voltage was higher than 2.1 V. Therefore, the phenol degradation rate in the PEC process reached a maximum when the additional applied voltage was 2.1 V. However, if the applied voltage in the PEC process was higher than 2.1 V, the degradation rate (k) of phenol would not increase with the increase of the applied voltage but decrease. The decreased k was due to the reallocation of the Hector Helmholtz layer and the space charge layer. Due to the reallocation, the number of photogenerated h^+-e^- pairs would be reduced. Additionally, the phenol at the high applied voltage could form polymers and adsorb on the surface of the SA-PDI film, which hindered the degradation of phenol [50–52]. Therefore, 2.1 V was regarded as the optimum applied voltage for phenol degradation under visible light irradiation. Most importantly, the SA-PDI film shows a superior degradation activity compared with the other reported catalysts (Fig. S8a online). Furthermore, total organic carbon (TOC) measurements were also carried out, and the results further confirm the strong degradation activity of the SA-PDI thin film during the PEC process (Fig. S8b online).

3.6. Stability of the SA-PDI film

The stability of the SA-PDI film for phenol degradation was also confirmed through a cyclic experiment (Fig. 4d), SEM images (Fig. S9a online), and XRD spectra (Fig. S9b online). The SA-PDI film was recycled and reused 3 times under visible light irradiation and an applied voltage (2.1 V) in the PEC degradation. The PEC degradation performance during the 3 reaction cycles maintained a similar level. Additionally, no differences have been found in the SEM images and XRD spectra of the SA-PDI thin film before and after catalysis, indicating that the crystallinity and small d-spacing of the π-π stacking of SA-PDI thin film did not change during the PEC reaction. These results indicated that the SA-PDI film possessed not only high photoelectrocatalytic activity but also good stability.

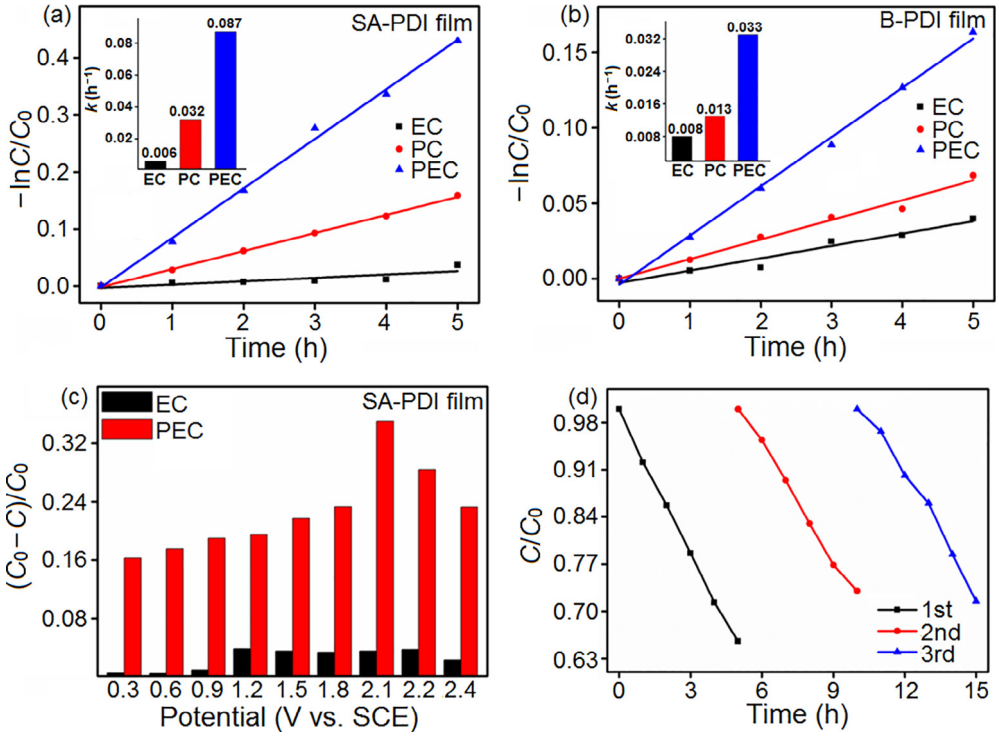

Fig. 4. (Color online) Photoelectooxidation performance of phenol. The first order kinetics curve fitting for EC, PC and PEC degradation of phenol by the SA-PDI film (a) or B-PDI (b) film (visible light, 2.1 V applied voltage). (c) PEC and EC degradation of phenol (5 ppm) on the SA-PDI film at various applied voltages in Na_2SO_4 solution (0.1 mol/L). (d) The cyclic performance test for the phenol degradation of the SA-PDI film under the PEC process.

3.7. Mechanistic analysis

The results of the above photoelectrochemical tests and phenol degradation experiments showed that the PEC degradation was higher than those of the PC and EC processes. The photocatalytic activity mainly relied on the separation efficiency of photogenerated current carriers [53] and electron transfer. In the PEC process, the applied voltage may generate more radical species with strong oxidation capabilities. The electron spin resonance (ESR) spin-trapping measurements were used to detect radicals in the reaction systems. The presence of ·OH or $\cdot O_2^-$ could be reflected by the DMPO, which could act as a spin trap. The ESR spectrometer could be applied to detect the signal responses of ·OH and $\cdot O_2^-$. As shown in Fig. 5a, both the $\cdot O_2^-$ and ·OH signals could be observed. Concretely, it was difficult to observe the ESR signals of ·OH and $\cdot O_2^-$ in the dark. With visible light irradiation for approximately 4 min, the ESR signals appeared. The adsorbed O_2 in the water could scavenge photogenerated electrons and form $\cdot O_2^-$ (Eq. (2)). Furthermore, the ·OH was generated through Eqs. (3) and (4) [54,55].

$$e^- + O_2 \rightarrow \cdot O_2^- \quad (2)$$

$$2e^- + O_2 + 2H^+ \rightarrow H_2O_2 \quad (3)$$

$$H_2O_2 + \cdot O_2^- \rightarrow \cdot OH + OH^- + O_2 \quad (4)$$

Next, the active species and mechanism of the PEC process could also be investigated by the active species trapping experiment [56]. As shown in Fig. 5b, the changes in the PEC degradation efficiency with the addition of t-BuOH (hydroxyl radical scavenger) and KI (holes scavenger) could be easily observed. Specifically, the PEC degradation efficiency decreased slightly with the addition of t-BuOH, which indicated that the ·OH was not the main active species during the PEC process. Significantly, the PEC degradation efficiency was obviously suppressed with the addition of KI, indicating that h^+ was the main oxidative species. The fluorescence spectra were also be used to measure the contents of ·OH generated in the PC, EC and PEC processes, respectively. Terephthalic acid (TA) could be regarded as a stable fluorescence probe for capturing the ·OH and generating 2-hydroxy terephthalic acid (TAOH). The TAOH could be excited at 315 nm and showed emission of unique fluorescence at approximately 435 nm [57,58]. The fluorescence spectra of TAOH appeared to show striking variations in the three types of processes (Fig. 5c). Specifically, the fluorescence intensity in EC was higher than in the PC process, which indicated that the applied voltage could produce more active ·OH. Thus, the phenol degradation during the PEC process was attributed to the synergistic reaction with visible light irradiation and the applied voltage.

Furthermore, the degradation pathway of phenol was recorded and confirmed by the HPLC system (Fig. S10a online). The peaks at 3.031, 2.361, 1.958, 1.737, and 0.965 min correspond to phenol, *p*-benzoquinone, hydroquinone, phosphate buffer and maleic acid [33]. Other more emerging contaminants (2,4-dichlorophenol and ciprofloxacin) were also used to evaluate the PEC activity of the SA-PDI film (Fig. S10b online). The degradation rate of ciprofloxacin by the SA-PDI film was 0.89 h^{-1}. The ciprofloxacin (10 ppm) was oxidized to H_2O and CO_2 by the PEC process after 2.5 h.

4. Conclusions

SA-PDI nanowire was further used to obtain the SA-PDI film. The SA-PDI film was applied to the PEC degradation of phenol. The synergistic effect of photo- and electro- could promote and optimize each other during the PEC degradation process. The applied bias improved the photogenerated h^+-e^- separation efficiency and generated more active species, and in the meantime,

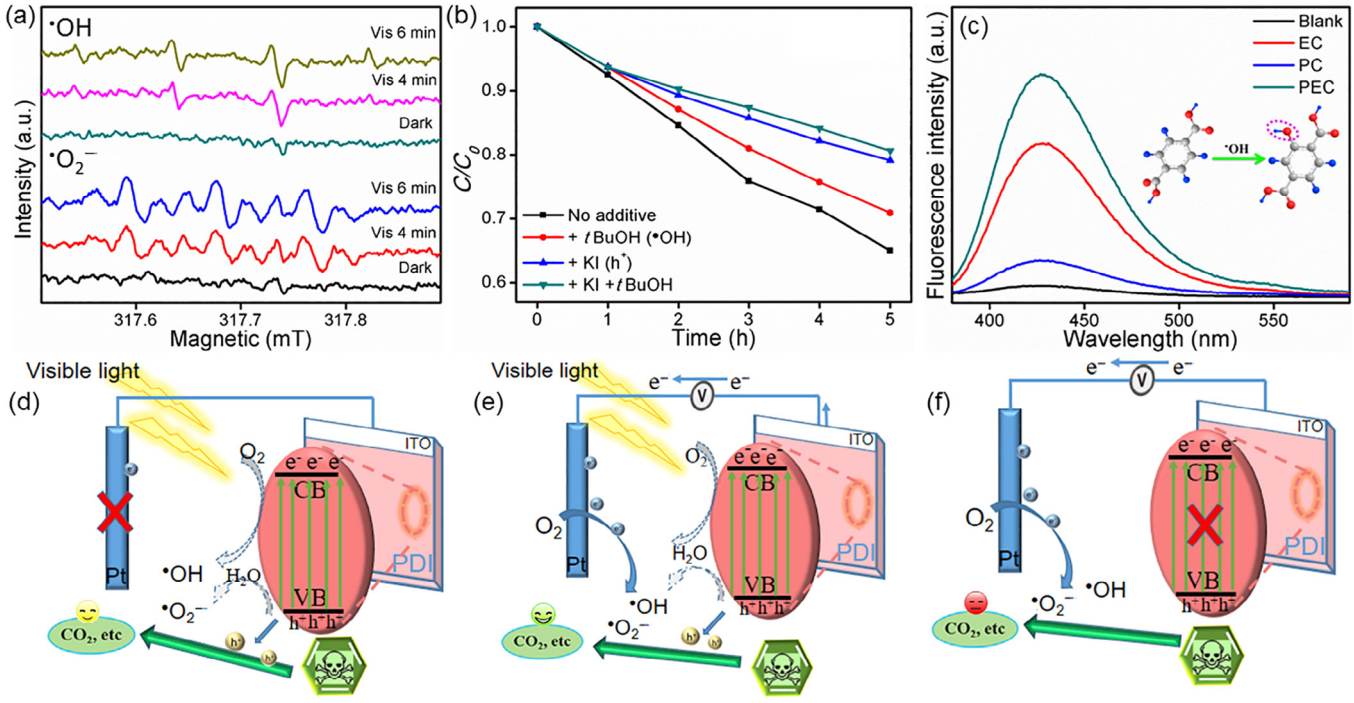

Fig. 5. (Color online) Mechanism of the SA-PDI film degraded phenol. (a) ESR spectra of the SA-PDI film in DMSO solvent detected $\cdot O_2^-$ and that in water detected ·OH. (b) Plots of photogenerated carriers trapped by the PEC process by the SA-PDI film under visible light ($\lambda > 420$ nm) and an applied voltage (2.1 V). (c) Fluorescence emission intensity peaks related to the amount of ·OH produced through the PC, EC and PEC processes after 2 h of visible light irradiation at an applied voltage of 2.1 V. Schematic description of the mechanism for the PC (d), PEC (e) and EC (f) processes for the oxidation of phenol.

the visible light irradiation could generate a promoting effect on EC degradation. Thereby, the synergistic effect between EC and PC of the SA-PDI film not only significantly enhanced the phenol degradation efficiency but could also be developed to meet the increasing demand for practical applications.

Conflict of interest

The authors declare that they have no conflict of interest.

Acknowledgments

This work was partly supported by the National Natural Science Foundation of China (21673126, 21437003, 21761142017, and 21621003) and Collaborative Innovation Center for Regional Environmental Quality.

Author contributions

Yongfa Zhu proposed and designed the research. Hong Miao performed the research. Jun Yang and Guilong Peng participated in part of experiments. Hong Miao and Huiquan Li analyzed the data and co-wrote the manuscript. All authors discussed the results and commented on the manuscript.

Appendix A. Supplementary data

Supplementary data to this article can be found online at https://doi.org/10.1016/j.scib.2019.05.006.

References

[1] Shi S, Qu Y, Ma F, et al. Bioremediation of coking wastewater containing carbazole, dibenzofuran and dibenzothiophene by immobilized naphthalene-cultivated Arthrobacter sp. W1 in magnetic gellan gum. Bioresour Technol 2014;166:79–86.
[2] Zhang WH, Wei CH, An GF. Distribution, partition and removal of polycyclic aromatic hydrocarbons (PAHs) during coking wastewater treatment processes. Environ Sci 2015;17:975–84.
[3] Ioannou-Ttofa L, Michael-Kordatou I, Fattas SC, et al. Treatment efficiency and economic feasibility of biological oxidation, membrane filtration and separation processes, and advanced oxidation for the purification and valorization of olive mill wastewater. Water Res 2017;114:1–13.
[4] Zhang H, Zhao LX, Geng FL, et al. Carbon dots decorated graphitic carbon nitride as an efficient metal-free photocatalyst for phenol degradation. Appl Catal B Environ 2016;180:656–62.
[5] Fang HP, Liang DW, Zhang T. Anaerobic treatment of phenol in wastewater under thermophilic condition. Water Res 2006;40:427–34.
[6] Pérez M, Torrades F. Removal of organic contaminants in paper pulp treatment effluents under Fenton and photo-Fenton conditions. Appl Catal B Environ 2002;36:63–74.
[7] Santos A, Yustos P, Gomis S. Reaction network and kinetic modeling of wet oxidation of phenol catalyzed by activated carbon. Chem Eng Sci 2006;61:2457–67.
[8] Duan XG, Sun HQ, Wang YX, et al. *N*-doping-induced nonradical reaction on single-walled carbon nanotubes for catalytic phenol oxidation. ACS Catal 2015;5:553–9.
[9] Sillanpää ME, Kurniawan TA, Lo W. Degradation of chelating agents in aqueous solution using advanced oxidation process (AOP). Chemosphere 2011;83:1443–60.
[10] Aydin A, Altinbas M, Sevimli M, et al. Advanced treatment of high strength opium alkaloid industry effluents. Water Sci Technol 2002;46:323–30.
[11] Mahiroglu A, Tarlan-Yel E, Sevimli MF. Treatment of combined acid mine drainage (AMD)-Flotation circuit effluents from copper mine via Fenton's process. J Hazard Mater 2009;166:782–7.
[12] Han S, Hu L, Liang Z, et al. One-step hydrothermal synthesis of 2D hexagonal nanoplates of α-Fe_2O_3/graphene composites with enhanced photocatalytic activity. Adv Funct Mater 2014;24:5719–27.
[13] Sotelo-Vazquez C, Quesada-Cabrera R, Ling M, et al. Evidence and effect of photogenerated charge transfer for enhanced photocatalysis in WO_3/TiO_2 heterojunction films: a computational and experimental study. Adv Funct Mater 2017;27:1605413.
[14] Fakhri P, Jaleh B, Nasrollahzadeh M. Synthesis and characterization of copper nanoparticles supported on reduced graphene oxide as a highly active and recyclable catalyst for the synthesis of formamides and primary amines. J Mol Catal A: Chem 2014;383:17–22.
[15] Ochiai T, Fujishima A. Photoelectrochemical properties of TiO_2 photocatalyst and its applications for environmental purification. J Photochem Photobiol C 2012;13:247–62.
[16] Zhang Y, Wang Q, Lu J, et al. Synergistic photoelectrochemical reduction of Cr (VI) and oxidation of organic pollutants by g-C_3N_4/TiO_2-NTs electrodes. Chemosphere 2016;162:55–63.
[17] Zhai C, Zhu M, Ren F, et al. Enhanced photoelectrocatalytic performance of titanium dioxide/carbon cloth based photoelectrodes by graphene modification under visible-light irradiation. J Hazard Mater 2013;263:291–8.
[18] Sun H, Li G, Nie X, et al. Systematic approach to in-depth understanding of photoelectrocatalytic bacterial inactivation mechanisms by tracking the decomposed building blocks. Environ Sci Technol 2014;48:9412–9.
[19] Li G, Liu X, Zhang H, et al. In situ photoelectrocatalytic generation of bactericide for instant inactivation and rapid decomposition of Gram-negative bacteria. J Catal 2011;277:88–94.
[20] Nie X, Li G, Gao M, et al. Comparative study on the photoelectrocatalytic inactivation of *Escherichia coli* K-12 and its mutant *Escherichia coli* BW25113 using TiO_2 nanotubes as a photoanode. Appl Catal B Environ 2014;147:562–70.
[21] Baram N, Starosvetsky D, Starosvetsky J, et al. Enhanced photo-efficiency of immobilized TiO_2 catalyst via intense anodic bias. Electrochem Commun 2007;9:1684–8.
[22] Zhang Y, Xiong X, Han Y, et al. Photoelectrocatalytic degradation of recalcitrant organic pollutants using TiO_2 film electrodes: an overview. Chemosphere 2012;88:145–54.
[23] Feng XJ, Zhai J, Jiang L. The fabrication and switchable superhydrophobicity of TiO_2 nanorod films. Angew Chem Int Ed 2005;44:5115–8.
[24] Li D, Jia JL, Zheng T, et al. Construction and characterization of visible light active Pd nano-crystallite decorated and C-N-S-co-doped TiO_2 nanosheet array photoelectrode for enhanced photocatalytic degradation of acetylsalicylic acid. Appl Catal B Environ 2016;188:259–71.
[25] Su YF, Wang GB, Kuo DTF, et al. Photoelectrocatalytic degradation of the antibiotic sulfamethoxazole using TiO_2/Ti photoanode. Appl Catal B Environ 2016;186:184–92.
[26] Zheng Q, Lee C. Visible light photoelectrocatalytic degradation of methyl orange using anodized nanoporous WO_3. Electrochim Acta 2014;115:140–5.
[27] Murcia-López S, Fàbrega C, et al. Tailoring multilayered $BiVO_4$ photoanodes by pulsed laser deposition for water splitting. ACS Appl Mater Interfaces 2016;8:4076–85.
[28] Gromboni MF, Coelho D, Mascaro LH, et al. Enhancing activity in a nanostructured $BiVO_4$ photoanode with acoating of microporous Al_2O_3. Appl Catal B Environ 2017;200:133–40.
[29] Hong SJ, Lee S, Jang JS, et al. Heterojunction $BiVO_4/WO_3$ electrodes for enhanced photoactivity of water oxidation. Energy Environ Sci 2011;4:1781–7.
[30] Zhang M, Pu WH, Pan SC, et al. Photoelectrocatalytic activity of liquid phase deposited a-Fe_2O_3 films under visible light illumination. J Alloy Compd 2015;648:719–25.
[31] Datar A, Balakrishnan K, Zang L. One-dimensional self-assembly of a water soluble perylene diimide molecule by pH triggered hydrogelation. Chem Commun 2013;49:6894–6.
[32] Shuai C, Slattum P, Wang C. Self-assembly of perylene imide molecules into 1D nanostructures: methods, morphologies, and applications. Chem Rev 2015;115:11967–98.
[33] Liu D, Wang J, Bai X. Self-assembled PDINH supramolecular system for photocatalysis under visible light. Adv Mater 2016;28:7284–90.
[34] Wang J, Shi W, Liu D, et al. Supramolecular organic nanofibers with highly efficient and stable visible light photooxidation performance. Appl Catal B Environ 2017;202:289–97.
[35] Zeng L, Liu T, He C. Organized aggregation makes insoluble perylene diimide efficient for the reduction of aryl halides via consecutive visible light-induced electron-transfer processes. J Am Chem Soc 2016;138:3958–61.
[36] Zhang Z, Wang J, Liu D. Highly efficient organic photocatalyst with full visible light spectrum through π-π stacking of TCNQ-PTCDI. ACS Appl Mater Interfaces 2016;8:30225–31.
[37] Wang H, Zhao L. Novel hydrogen bonding composite based on copper phthalocyanine/perylene diimide derivatives p-n heterojunction with improved photocatalytic activity. Dyes Pigments 2017;137:322–8.
[38] Wang HL, Zhang LS, Wang XC. Semiconductor heterojunction photocatalysts: design, construction, and photocatalytic performances. Chem Soc Rev 2014;43:5234–44.
[39] Zhang K, Wang J, Jiang WJ, et al. Self-assembled perylene diimide based supramolecular heterojunction with Bi_2WO_6 for efficient visible-light-driven photocatalysis. Appl Catal B Environ 2018;232:175–81.
[40] Wei W, Liu D, Wei Z, et al. Short-range π-π stacking assembly on P25 TiO_2 nanoparticles for enhanced visible-light photocatalysis. ACS Catal 2017;7:652–63.
[41] Chen S, Li YX, Wang CY. Visible-light-driven photocatalytic H_2 evolution from aqueous suspensions of perylene diimide dye-sensitized Pt/TiO_2 catalysts. RSC Adv 2015;5:15880–5.
[42] Liu D, Zhou J, Wang JQ, et al. Enhanced visible light photoelectrocatalytic degradation of organic contaminants by F and Sn co-doped TiO_2 photoelectrode. Chem Eng J 2018;344:332–41.

[43] Lin J, Zong RL, Zhou M, et al. Photoelectric catalytic degradation of methylene blue by C_{60}-modified TiO_2 nanotube array. Appl Catal B Environ 2009;89:425–31.
[44] Leng WH, Zhang Z, Zhang JQ, et al. Investigation of the kinetics of a TiO_2 photoelectrocatalytic reaction involving charge transfer and recombination through surface states by electrochemical impedance spectroscopy. J Phys Chem B 2005;109:15008–23.
[45] Muna GW, Tasheva N, Swain GM. Electro-oxidation and amperometric detection of chlorinated phenols at boron-doped diamond electrodes: a comparison of microcrystalline and nanocrystalline thin films. Environ Sci Technol 2004;38:3674–82.
[46] Simond O, Schaller V, Comninellis C. Theoretical model for the anodic oxidation of organics on metal oxide electrodes. Electrochim Acta 1997;42:2009–12.
[47] Miao H, Yang J, Wei YX, et al. Visible-light photocatalysis of PDI nanowires enhanced by plasmonic effect of the gold nanoparticles. Appl Catal B Environ 2018;239:61–7.
[48] Liang FF, Zhu YF. Enhancement of mineralization ability for phenol via synergetic effect of photoelectrocatalysis of g-C_3N_4 film. Appl Catal B Environ 2016;180:324–9.
[49] Kuang P, Ran J, Liu Z, et al. Enhanced photoelectrocatalytic activity of BiOI nanoplate – zinc oxide nanorod p–n heterojunction. Chem Eur J 2015;21:15360–8.
[50] Pelegrini R, Reyes J, Duran N, et al. Photoelectrochemical degradation of lignin. J Appl Electrochem 2000;30:953–8.
[51] Wang YJ, Xu J, Zong WZ, et al. Enhancement of photoelectric catalytic activity of TiO_2 film via polyaniline hybridization. J Solid State Chem 2011;184:1433–8.
[52] Zhao X, Zhu YF. Synergetic degradation of rhodamine B at a porous $ZnWO_4$ film electrode by combined electro-oxidation and photocatalysis. Environ Sci Technol 2006;40:3367–72.
[53] Cao D, Wang YB, Qiao M, et al. Enhanced photoelectrocatalytic degradation of norfloxacin by an $Ag_3PO_4/BiVO_4$ electrode with low bias. J Catal 2018;360:240–9.
[54] Daghrir R, Drogui P, Robert D. Photoelectrocatalytic technologies for environmental applications. J Photochem Photobiol A 2012;238:41–52.
[55] Wei Z, Liang FF, Liu YF, et al. Photoelectrocatalytic degradation of phenol-containing wastewater by TiO_2/g-C_3N_4 hybrid heterostructure thin film. Appl Catal B Environ 2017;201:600–6.
[56] Xu TG, Zhang LW, Cheng HY, et al. Significantly enhanced photocatalytic performance of ZnO via graphene hybridization and the mechanism study. Appl Catal B Environ 2011;101:382–7.
[57] Miao H, Zhong D, Zhou ZN, et al. Papain-templated Cu nanoclusters: assaying and exhibiting dramatic antibacterial activity cooperating with H_2O_2. Nanoscale 2015;7:19066–72.
[58] Ishibashi K, Fujishima A, Watanabe T, et al. Detection of active oxidative species in TiO_2 photocatalysis using the fluorescence technique. Electrochem Commun 2000;2:207–10.

Hong Miao is a Ph.D. student at the Department of Chemistry, Tsinghua University. He received his B.S. degree from the College of Pharmaceutical Sciences, Southwest University. His research focuses on the design and fabrication of organic photocatalysts and their application for the environmental pollution control and the resource utilization of solar energy.

Yongfa Zhu received his B.S. degree in 1985 from Nanjing University and obtained his M.S. degree in 1988 from the Peking University. He has studied and worked at Tsinghua University since 1992 and received his Ph.D. degree in 1995. He is currently a full professor at Tsinghua University. His current research focuses on photocatalysis, environmental catalysis and nanomaterials.